Medicinal Chemistry Research (2019) 28:485–497
https://doi.org/10.1007/s00044-019-02293-w

MEDICINAL CHEMISTRY RESEARCH

ORIGINAL RESEARCH

New indole and indazole derivatives as potential antimycobacterial agents

Violina T. Angelova[1] · Tania Pencheva[2] · Nikolay Vassilev[3] · Rumyana Simeonova[4] · Georgi Momekov[4] · Violeta Valcheva[5,6]

Received: 21 October 2018 / Accepted: 18 January 2019 / Published online: 8 February 2019

Abstract

The study reports on the synthesis and in vitro assessment of the antimycobacterial activity of a series of new indole- and indazole-based aroylhydrazones evaluated against *Mycobacterium tuberculosis* H37Rv. Isoniazide and ethambutol were used as reference drugs. The most active compounds **3a** (MIC 0.4412 μM) and **3e** (MIC 0.3969 μM) demonstrated excellent antimycobacterial activity, a very low toxicity against the human embryonic kidney cell line HEK-293T and high selectivity index values (SI = 633.49 and SI > 1978.83, respectively). Importantly, the oral administration of compound **3e** at the highest dose of 2000 mg/kg b.w. resulted in no mortalities or evidence of adverse effects, implying that compound **3e** is nontoxic. The other derivatives with an indole and indazole scaffold also exhibited high antimycobacterial activity with exception of indole derivatives with Br substituents at the 5th position which exhibited activity weaker than that of ethambutol. The molecular docking investigations performed in an enoyl-ACP reductase (InhA) displayed good docking scores and promising insights on possible interactions with the InhA receptor.

Graphical Abstract

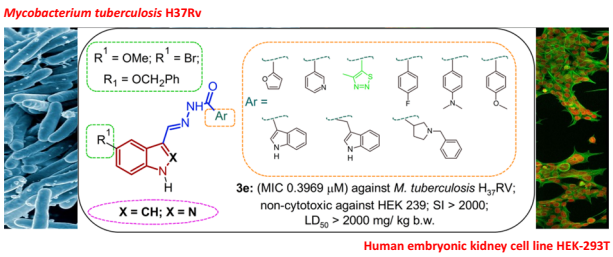

Supplementary information The online version of this article (https://doi.org/10.1007/s00044-019-02293-w) contains supplementary material, which is available to authorized users.

✉ Violina T. Angelova
violina_stoyanova@abv.bg
violina@pharmfac.net

[1] Department of Chemistry, Faculty of Pharmacy, Medical University of Sofia, 2, Dunav St., Sofia 1000, Bulgaria

[2] Institute of Biophysics and Biomedical Engineering, Bulgarian Academy of Sciences, 105, Acad. G. Bonchev St., Sofia 1113, Bulgaria

[3] Laboratory of Nuclear Magnetic Resonance, Institute of Organic Chemistry with Centre of Phytochemistry, Bulgarian Academy of Sciences, 9, Acad. G. Bonchev St., Sofia 1113, Bulgaria

[4] Department of Pharmacology, Pharmacotherapy and Toxicology, Faculty of Pharmacy, Medical University-Sofia, 2, Dunav St., Sofia 1000, Bulgaria

[5] Institute of Microbiology, Bulgarian Academy of Sciences, 26, Acad. G. Bonchev St., Sofia 1113, Bulgaria

[6] In Vitro Laboratory for Evaluation of Biological Activity and Toxicity, Sofia Tech Park, 111 TsarigradskoShose Blvd., Sofia, Bulgaria

Keywords Antimycobacterial activity · Cytotoxicity · Indazole · Indole · InhA · LD_{50} · Molecular docking

Introduction

The search for effective and nontoxic chemotherapeutic agents for tuberculosis (TB) treatment is a very important issue worldwide. It has been intensified by the striving to overcome the increasing problem in most of the countries (da Silva et al. 2017) related to the occurrence of MDR-TB (multidrug resistant TB) and associated with tuberculosis viral infections (human immunodeficiency virus (HIV) infection) which cause a number of inadequate effects of the first- and second-line anti-tuberculosis drugs. According to the World Health Organization (WHO), tuberculosis affects one-third of the world's population, with 10.4 million new cases in 2016 (10% among HIV co-infected individuals), 1.67 million deaths and 490,000 MDR plus an additional 110,000 rifampicin-resistant cases (World Health Organization 2018). The urgent improvement of new potent antitubercular drugs has four promising targets: FASII enoyl-acyl carrier protein reductase (InhA), transmembrane transport protein large (MmpL3), decaprenylphospho-beta-dribofuranose 2-oxidase (DprE1), and ubiquinol-cytochrome *C* reductase (QcrB) (Campaniço et al. 2018). A new and more efficient approach in the fight against tuberculosis is the development of compounds targeting directly InhA which do not require activation by KatG. In this aspect, the hydrazone derivatives turned to be effective and less hepatotoxic agents (Elhakeem et al. 2015). Furthermore, hydrazone derivatives are present in many bioactive molecules and display a wide variety of biological activities, such as anticancer (Peng et al. 2018; Parlar et al. 2018; Rudavath et al. 2018) anti-inflammatories (Poma et al. 2012), antimicrobial (Peng et al. 2018; Popiołek and Biernasiuk 2017; Popiołek et al. 2018), anticonvulsant (Dehestani et al. 2018; Ragavendran et al. 2007), antiviral (Şenkardeş et al. 2016), and antiprotozoal (Inam et al. 2014). Actually, among all the biological properties of the hydrazide–hydrazones, their antimycobacterial activity is the most frequently discussed in the scientific literature (Velezheva et al. 2016; Coelho et al. 2012; Cihan-Üstündağ and Çapan 2012; John et al. 2016; Angelova et al. 2017b).

The indole ring system has been another scaffold among the most-studied pharmacophore groups in drug research studies (North and Jackson 2018). It is present in the structure of many pharmacologically active products that exhibit antimycobacterial activity (Ashok et al. 2018; Negatu et al. 2017; Nyantakyi et al. 2018; Shirinzadeh et al. 2011; Yang et al. 2017; Yurttaş et al. 2017). Also, some indazole derivatives have been identified as attractive new classes of drug candidates against *Mycobacterium tuberculosis* (Park et al. 2016, Malapati and Dharmarajan 2018, Vidyacharan et al. 2017, Faidallah et al. 2013). Inspired by the antimycobacterial activity of the reported indole and indazole derivatives, we expand further this scaffold concept towards hydrazide–hydrazone derivatives. Structural modification efforts are directed to the identification of novel indole and indazole derivatives with hydrazide–hydrazone moiety as potent antimycobacterial agents.

Materials and methods

Chemistry

General

The melting points were determined using a Buchi 535 apparatus and Melting point meter M5000 apparatus. The Fourier-transform infrared spectroscopy (FTIR) spectra were recorded on a Nicolet IS10 FT-IR Spectrometer from Thermo Scientific (USA) using an attenuated total reflection (ATR) technique and FTIR spectrometer Bruker-Tenzor 27. All nuclear magnetic resonance (NMR) experiments were carried out on a BrukerAvance spectrometer II+600 MHz at 20 °C in dimethyl sulfoxide (DMSO)-d_6 as a solvent, using tetramethylsilane as an internal standard. The precise assignment of the ^{1}H and ^{13}C NMR spectra was accomplished by measurement of two-dimensional (2D) homonuclear correlation (correlation spectroscopy (COSY)), DEPT-135, and 2D inverse detected heteronuclear (C–H) correlations (heteronuclear single-quantum correlation spectroscopy (HMQC) and heteronuclear multiple-bond correlation spectroscopy (HMBC)). Mass spectra were measured on a Q Exactive Plus mass spectrometer (ThermoFisher Scientific) equipped with a heated electrospray ionization (HESI-II) probe (Thermo Scientific). All chemicals as well as compounds **1** and **2a–k** used for the synthesis were commercial products and used without further purification. The purity of the new compounds was checked by thin-layer chromatography (TLC) on silica gel 60 GF254 Merck pre-coated aluminum sheets, eluted by hexane–chloroform–acetone–methanol 4:3:2:1 (vol. parts); the spots were visualized under ultraviolet irradiation ($\lambda = 254$ nm).

General procedure for the synthesis of compounds 3a–k, 5l–m

To a solution of appropriate hydrazides **2a–m** (2.0 mmol) in absolute (abs.) ethanol a stirred solution of 5-metoxyindole-3-

carbaldehyde (2.0 mmol) **1a**, 5-bromoindole-3-carbaldehyde (2.0 mmol) **1b**, 5-benzyloxyindole-3-carbaldehyde (2.0 mmol) **1c**, or 5-metoxyindazole-3-carbaldehyde (2.0 mmol) **4** in abs. ethanol was added. The solution was refluxed for 2–3 h. The solid product formed was collected by filtration and recrystallized with ethanol.

Synthesis of indol and indazole containing aroylhydrazones

N′-[(*E*)-(5-methoxy-1*H*-indol-3-yl)methylidene]furan-2-carbohydrazide, 3a

Yield: 81%; m.p. 222–224 °C. FTIR(ATR) ν_{max}: 3266 NH, 3211 NH, 1641(*cis*), 1630(*trans*) C = O, 1607 C = N, 1572 C = C cm^{-1}; ^{1}H NMR (DMSO-d_6, 600 MHz): 1:0.23 mixture of conformers; signals for major *synperiplanar conformer* around the amide bond: δ 3.787 (s, 3H, OCH_3), 6.685 (dd, J = 1.6, 3.3 Hz, 1H, H-4'), 6.853 (dd, J = 2.5, 8.8 Hz, 3H, H-6), 7.232 (d, J = 3.3 Hz, 1H, H-5'), 7.335 (d, J = 8.7 Hz, 1H, H-7), 7.762 (d, J = 2.7 Hz, 1H, H-2), 7.819 (d, J = 2.3 Hz, 1H, H-4), 7.913 (brs, 1H, H-3'), 8.592 (s, 1H, H-8), 11.469 (brs, 1H, CONH), 11.513 (brs, 1H, NH) ppm. ^{13}C NMR (DMSO-d_6, 150 MHz): 55.75 (OCH_3), 104.67 (C-4), 111.88 (C-3), 112.41 (C-4'), 112.66 (C-6), 112.89 (C-7), 114.44 (C-5'), 125.42 (C-3a), 131.14 (C-2), 132.46 (C-7a), 145.62 (C-8), 145.77 (C-3'), 147.72 (C-1'), 154.20 (C=O), 154.87 (C-5) ppm. High-resolution mass spectrometry (HRMS) (electrospray ionization (ESI)) *m/z*: calcd: $[M + H]^+$ 284.10244. Found: $[M + H]^+$ 284.102968.

N′-[(*E*)-(5-methoxy-1*H*-indol-3-yl)methylidene]pyridine-3-carbohydrazide, 3b

Yield: 76%; m.p. 232–233 °C FTIR(ATR) ν_{max}: 3350 NH, 3270 NH, 1637 C = O, 1610 C = N, 1602 C = C; ^{1}H NMR (DMSO-d_6, 600 MHz): 1:0.19 mixture of conformers; signals for major *synperiplanar conformer* around the amide bond: δ 3.797 (s, 3H, OCH_3), 6.860 (dd, J = 2.6, 8.8 Hz, 1H, H-6), 7.346 (d, J = 8.8 Hz, 1H, H-7), 7.565 (ddd, J = 0.8, 4.8, 7.9 Hz, 1H, H-5'), 7.799 (d, J = 2.8 Hz, 1H, H-2), 7.845 (d, J = 2.5 Hz, 1H, H-4), 8.258 (ddd, J = 1.8, 2.2, 7.9 Hz, 1H, H-6'), 8.584 (s, 1H, H-8), 8.745 (dd, J = 1.6, 4.8 Hz, 1H, H-4'), 9.070 (1H, dd, J = 0.8, 2.3 Hz, 1H, H-2'), 11.500 (brd, J = 1.9 Hz, 1H, CONH), 11.692 (brs, 1H, NH) ppm. ^{13}C NMR (DMSO-d_6, 150 MHz): δ 55.38 (OCH_3), 104.19 (C-4), 111.36 (C-3), 112.40 (C-6), 112.57 (C-7), 123.66 (C-5'), 125.02 (C-3a), 129.82 (C-1'), 131.12 (C-2), 132.09 (C-7a), 135.35 (C-6'), 145.80 (C-8), 148.54 (C-2'), 151.97 (C-4'), 154.56 (C-5), 161.00 (C=O) ppm. HRMS (ESI) *m/z*: calcd: $[M + H]^+$ 312.114281. Found: $[M + H]^+$ 312.11343.

4-(Dimethylamino)-*N*′-[(*E*)-(5-methoxy-1*H*-indol-3-yl) methylidene]benzohydrazide, 3c

Yield: 77%; m.p. 160–161 °C. FTIR(ATR) ν_{max}: 3314 NH, 3215 NH, 1623 C=O, 1599 C=N; 1583 C=C cm^{-1}; ^{1}H NMR (DMSO-d_6, 600 MHz): 1:0.19 mixture of conformers; signals for major *synperiplanar conformer* around the amide bond: δ 2.991 (s, 6H, NCH_3), 3.794 (s, 3H, OCH_3), 6.756 (d, J = 8.8 Hz, 2H, H-3' and H-5'), 6.844 (dd, J = 2.3, 8.7 Hz, 1H, H-6), 7.326 (d, J = 8.7 Hz, 1H, H-7), 7.723 (d, J = 2.6 Hz, 1H, H-2), 7.820 (d, J = 8.8 Hz, 2H, H-2' and H-6'), 7.856 (d, J = 1.9 Hz, 1H, H-4), 8.574 (s, 1H, H-8), 11.218 (s, 1H, CONH), 11.401 (s, 1H, NH) ppm. ^{13}C NMR (DMSO-d_6, 150 MHz): δ 39.77 (NCH_3), 55.34 (OCH_3), 104.21 (C-4), 110.92 (C-3' and C-5'), 111.77 (C-3), 112.22 (C-6), 112.37 (C-7), 120.32 (C-1'), 125.01 (C-3a), 128.83 (C-2' and C-6'), 130.06 (C-2), 132.02 (C-7a), 143.68 (C-8), 152.24 (C-4'), 154.34 (C-5), 162.30 (C=O) ppm. HRMS (ESI) *m/z*: calcd: $[M+H]^+$ 337.165902. Found: $[M+H]^+$ 337.16517.

4-Methoxy-*N*′-[(*E*)-(5-methoxy-1*H*-indol-3-yl)methylidene] benzohydrazide, 3d

Yield: 86%; m.p. 259.1 °C. FTIR(ATR) ν_{max}: 3370 NH, 3256 NH, 1635 C=O, 1608 C=N, 1574 C=C cm^{-1}; ^{1}H NMR (DMSO-d_6, 600 MHz): 1:0.15 mixture of conformers; signals for major *synperiplanar conformer* around the amide bond: δ 3.796 (s, 3H, OCH_3), 3.833 (s, 3H, $PhOCH_3$), 6.852 (dd, J = 2.5, 8.8 Hz, 1H, H-6), 7.057 (d, J = 8.8 Hz, 2H, H-3' and H-5'), 7.334 (d, J = 8.7 Hz, 1H, H-7), 7.757 (d, J = 2.3 Hz, 1H, H-2), 7.854 (d, J = 2.3 Hz, 1H, H-4), 7.918 (d, J = 8.7 Hz, 2H, H-2' and H-6'), 8.587 (s, 1H, H-8), 11.394 (brs, 1H, CONH), 11.442 (brs, 1H, NH) ppm. ^{13}C NMR (DMSO-d_6, 150 MHz): δ 55.33 (OCH_3), 55.41 ($PhOCH_3$), 104.20 (C-4), 111.58 (C-3), 112.24 (C-6), 112.41 (C-7), 113.65 (C-3' and C-5'), 124.99 (C-3a), 126.14 (C-1'), 129.29 (C-2' and C-6'), 130.45 (C-2), 132.03 (C-7a), 144.55 (C-8), 154.39 (C-5), 161.68 (C-4'), 161.89 (C=O). HRMS (ESI) *m/z*: calcd: $[M+H]^+$ 324.134268. Found: $[M+H]^+$: 324.13366.

N′-[(E)-(5-methoxy-1*H*-indol-3-yl)methylidene]-4-methyl-1,2,3-thiadiazole-5-carbohydrazide, 3e

Yield: 92%; m.p. 260.2 °C. FTIR(ATR) ν_{max}: 3234 NH, 3137 NH, 1658, 1627 C=O, 1603 C=N 1585C=C cm^{-1}; ^{1}H NMR (DMSO-d_6, 600 MHz): 1:0.07 mixture of conformers; signals for major *synperiplanar conformer* around the amide bond: δ 2.970 (s, 3H, CH_3), 3.828 (s, 3H, OCH_3), 6.876 (dd, J = 2.5, 8.8 Hz, 1H, H-6), 7.381 (d, J = 8.8 Hz, 1H, H-7), 7.697 (d, J = 2.3 Hz, 1H, H-4), 7.907 (d, J = 2.9 Hz,

1H, H-2), 8.382 (s, 1H, H-8), 11.706 (brs, 1H, NH), 12.022 (brs, 1H, CONH) ppm. ^{13}C NMR (DMSO-d_6, 150 MHz): 15.26 (CH_3), 55.83 (OCH_3), 102.67 (C-4), 110.92 (C-3), 113.53 (C-6 and C-7), 124.44 (C-3a), 132.44 (C-7a), 133.30 (C-2), 136.91 (C-1'), 144.16 (C-8), 155.20 (C-5), 159.42 (C=O), 163.05 (C-5') ppm. HRMS (ESI) *m/z*: calcd: $[M+H]^+$ 316.08565. Found: $[M+H]^+$ 316.086271.

1-Benzyl-*N*′-[(E)-(5-methoxy-1*H*-indol-3-yl)methylidene] pyrrolidine-3-carbohydrazide, 3f

Yield: 78%.; m.p. 136–137 °C. FTIR(ATR) ν_{max}: 3482 NH, 3184 NH, 1647 C=O, 1622 C=N, 1582C=C; ^{1}H NMR (600 MHz, DMSO-d_6) 1:0.40 mixture of conformers; signals for major *synperiplanar* conformer around the amide bond: δ 2.090–2.145 (m, 1H, b-CH_2-4-H-pyrrolidine), 2.412–2.462 (m, 1H, a-CH_2-5-H-pyrrolidine), 2.525 (dd, J = 7.5, 8.9 Hz, 1H, a-CH_2-2-H-pyrrolidine), 2.613–2.656 (m, 1H, b-CH_2-5-H-pyrrolidine), 3.037 (t, J = 8.8 Hz, 1H, b-CH_2-2-H-pyrrolidine), 3.546 (d, J = 13.1 Hz, 1H a-CH_2-benzyl), 3.602 (d, J = 13.1 Hz, 1H, b-CH_2-benzyl), 3.764 (s, 3H, OCH_3), 3.775–3.829 (m, 1H, CH-3-pyrrolidine), 6.818 (dd, J = 2.5, 8.8 Hz, 1H, H-6-indole), 7.206 (m, 1H, *p*-phenyl), 7.282–7.322 (m, 4H, *m,o*-phenyl), 7.311 (d, J = 8.8 Hz, 1H, H-7-indole), 7.625 (d, J = 2.5 Hz, 1H, H-4-indole), 7.677 (d, J = 2.7 Hz, 1H, H-2-indole), 8.122 (s, 1H, CH=N), 10.946 (brs, 1H, NHCO), 11.372 (brs, 1H, NH); ^{13}C NMR (151 MHz, DMSO-d_6) signals for major *synperiplanar conformer* around the amide bond: δ 26.61 (C-4-pyrrolidine), 39.52 (C-3-pyrrolidine), 53.77 (C-5-pyrrolidine), 54.93 (CH_3O), 56.65 (C-2-pyrrolidine), 59.43 (CH_2-benzyl), 102.76 (C-4-indole), 111.32 (C-3-indole), 112.58 (C-6-indole), 112.59 (C-7-indole), 124.51 (C-3a-indole), 126.78 (*o*-phenyl), 128.15 (*p*-phenyl), 128.40 (*m*-phenyl), 130.34 (C-2-indole), 131.87 (C-7a-indole), 139.14 (*ipso*-phenyl), 140.14 (CH=N), 154.33 (C-5-indole), 174.35 (C=O). HRMS (ESI) m/z: calcd: $[M+H]^+$ 377.197202; Found $[M+H]^+$: 377.19643.

N′-[(*E*)-(5-bromo-1*H*-indol-3-yl)methylidene]-4-fluorobenzohydrazide, 3g

Yield: 72%; m.p. 223–226 °C. FTIR(ATR) ν_{max}: 3450 NH, 3179 NH, 1634 C=O, 1601 C=N, 1595 C=C; ^{1}H NMR (600 MHz, DMSO-d_6) δ 7.336 (dd, J = 2.03, 8.58 Hz, 1H, H-6), 7.355–7.394 (m, 2H, H-3',5'), 7.427 (d, J = 8.59 Hz, 1H, H-7), 7.909(d, J = 2.66 Hz, 1H, H-2), 7.984–8.017 (m, 2H, H-2',6'), 8.465 (d, J = 1.95 Hz, 1H, H-4), 8.586 (s, 1H, H-8), 11.619 (brs, 1H, CONH), 11.796 (brs, 1H, NH); ^{13}C NMR δ (151 MHz, DMSO-d_6) δ 111.34 (C-3), 113.14 (C-5), 113.94 (C-7), 115.43 (d, J = 21.8 Hz, C-3',5'), 124.20 (C-4), 125.21 (C-6), 126.00 (C-3a), 130.17 (d, J = 9.0 Hz, C-2',6'), 130.37 (d, J = 2.9 Hz, C-1'), 131.84 (C-2), 135.81 (C-7a), 144.58 (C-8), 161.52 (C=O), 163.99 (d, J = 248.95 Hz). HRMS (ESI) *m/z*: calcd $[M+H]^+$ 360.014222; Found $[M+H]^+$: 360.01381.

N′-[(*E*)-(5-bromo-1*H*-indol-3-yl)methylidene]pyridine-3-carbohydrazide, 3h

Yield: 92%; m.p. 303.1 °C. FTIR(ATR) ν_{max}: 3419 NH, 3142 NH, 1648 C=O, 1604 C=N, 1595C=C; ^{1}H NMR (600 MHz, DMSO-d_6) 1:0.2 mixture of conformers; signals for major *synperiplanar conformer* around the amide bond: δ 7.34 (dd, J = 2.00, 8.60 Hz, H-6), 1H, 7.43 (dd, J = 0.60, 8.60 Hz, 1H, H-7), 7.57 (ddd, J = 0.90, 4.80, 7.90 Hz, 1H, H-5-pyr), 7.93 (s, 1H, H-2), 8.26 (ddd, J = 1.70, 2.30, 7.90 Hz, 1H, H-4-pyr), 8.46 (dd, J = 0.6, 2.00 Hz, 1H, H-4), 8.59 (s, 1H, H-8), 8.76 (dd, J = 1.70, 4.80 Hz, 1H, H-6-pyr), 9.08 (dd, J = 0.90, 2.30 Hz, 1H, H-2-pyr), 11.77 (brs, 1H, CONH), 11.82 (brs, 1H, NH) ppm; ^{13}C NMR (151, MHz, DMSO-d_6) signals for major *synperiplanar conformer* around the amide bond: δ 111.21 (C-3), 113.21 (C-5), 113.98 (C-7), 123.62 (C-5-pyr), 124.18 (C-4), 125.25 (C-6), 126.00 (C-3a), 129.63 (C-3-pyr), 132.12 (C-2), 135.33 (C-4-pyr), 135.87 (C-7a), 145.18 (C-8), 148.52 (C-2-pyr), 152.03 (C-6-pyr), 161.18 (C=O). HRMS (ESI) *m/z*: calcd $[M+H]^+$ 343.01892; Found $[M+H]^+$: 343.01853.

N′-[(*E*)-(5-bromo-1*H*-indol-3-yl)methylidene]-1*H*-indole-3-carbohydrazide, 3i

Yield: 69%; m.p. 178–180 °C with decomp. FTIR(ATR) ν_{max}: 3395 NH, 3150 NH, 1631 C=O, 1602 C=N, 1580C=C; ^{1}H NMR (600 MHz, DMSO-d_6, 373 K), δ 7.145 (ddd, J = 1.1, 6.9, 7.9 Hz, 1H, H-5'), 7.189 (ddd, J = 1.1, 6.9, 8.1 Hz, 1H, H-6'), 7.315 (dd, J = 2.1, 8.6 Hz, 1H, H-6), 7.421 (dd, J = 0.7, 8.6 Hz, 1H, H-7), 7.479 (ddd, J = 0.9, 1.1, 8.1 Hz, 1H, H-7'), 7.741 (d, J = 2.7 Hz, 1H, H-2), 8.164 (d, J = 2.8 Hz, 1H, H-2'), 8.231 (d, J = 1.1, 7.9 Hz, 1H, H-4'), 8.435 (d, J = 2.1 Hz, 1H, H-4), 8.558 (s, 1H, H-8), 10.701 (s, 1H, NHCO), 11.407 (s, 2H, NH). ^{13}C NMR (151 MHz, DMSO-d_6) δ 108.98 (C-3'), 111.24 (C-7'), 111.47 (C-3), 112.45 (C-5), 113.16 (C-7), 119.89 (C-5'), 120.71 (C-4'), 121.45 (C-6'), 123.40 (C-4), 124.44 (C-6), 125.81 (C-3a), 126.27 (C-3a'), 128.09 (C-2'), 129.58 (C-2), 135.39 (C-7a), 135.73 (C-7a'), 141.13 (C-8), 161.55 (C=O). HRMS (ESI) *m/z*: calcd. $[M+H]^+$ 381.034542; Found $[M+H]^+$: 381.03418.

N′-[(E)-(5-bromo-1*H*-indol-3-yl)methylidene]-2-(1*H*-indol-3-yl)acetohydrazide,3j

Yield 69%; m.p. 250–251 °C with decomp. FTIR(ATR) ν_{max}: 3414 NH, 3377 NH 3125 NH, 1665 C=O, 1615 C=N, 1583C=C; ^{1}H NMR (600 MHz, DMSO-d_6) 1:0.84

mixture of conformers; signals for major synperiplanar conformer around the amide bond: δ 4.107 (s, 2H, CH2), 6.958 (ddd, J = 0.90, 7.04, 7.90 Hz, 1H, H-6-ind), 7.058 (ddd, J = 1.10, 7.04, 8.10 Hz, 1H, H-5-ind), 7.279 (d, J = 2.34 Hz, 1H, H-2-ind), 7.301 (dd, J = 2.00, 8.60 Hz, 1H, H-6-Br-ind), 7.337 (ddd, J = 0.90, 1.10, 8.10 Hz, 1H, H-4-ind), 7.428 (d, J = 8.60 Hz, 1H, H-7-Br-ind), 7.648 (ddd, J = 0.90, 1.10, 7.90 Hz, 1H, H-7-ind), 7.848 (d, J = 3.10 Hz, 1H, H-2-Br-ind), 8.178 (s, 1H, CH=N-NH), 8.426 (d, J = 2.00 Hz, 1H, H-4-Br-ind), 10.897 (s, 1H, NH-ind), 11.078 (brs, 1H, CONH), 11.731 (d, J = 3.10 Hz, 1H, NH-Br-ind); ^{13}C NMR (151 MHz, DMSO-d_6) signals for major synperiplanar conformer around the amide bond: δ 28.90 (CH2), 108.27 (C-3-ind), 111.16 (C-3-Br-ind), 111.33 (C-4-ind), 113.05 (C-5-Br-ind), 114.03 (C-7-Br-ind), 118.39 (C-6-ind), 118.70 (C-7-ind), 120.97 (C-5-ind), 123.65 (C-2-ind), 123.87 (C-4-Br-ind), 125.07 (C-6-Br-ind), 125.82 (C-3a-Br-ind), 127.48 (C-3a-ind), 131.37 (C-2-Br-ind), 135.79 (C-7a-Br-ind), 136.04 (C-7a-ind), 139.47 (CH=N-NH), 171.87 (C=O). HRMS (ESI) *m/z*: calcd $[M+H]^+$ 395.050193; Found $[M+H]^+$: 395.04994.

N′-{(E)-[5-(benzyloxy)-1*H*-indol-3-yl]methylidene}furan-2-carbohydrazide, 3k

Yield: 76%; m.p. 128–130 °C. FTIR(ATR) ν_{max}: 3397 NH, 3216 NH, 1642 C=O, 1609 C=N, 1582C=C; ^{1}H NMR (DMSO-d_6, 600 MHz): 1:0.22 mixture of conformers; signals for major *synperiplanar conformer* around the amide bond: δ 5.110 (s, 2H, CH_2), 6.689 (d, J = 1.4 Hz, 1H, H-4'), 6.920 (dd, J = 2.2, 8.7 Hz, 1H, H-6), 7.243 (d, J = 3.2 Hz, 1H, H-3'), 7.319 (t, J = 7.5 Hz, 1H, H-4"), 7.334 (d, J = 8.6, 1H, H-7), 7.389 (t, J = 7.5 Hz, 1H, H-3" and H-5"), 7.541 (d, J = 7.4 Hz, 1H, H-2" and H-6"), 7.764 (d, J = 2.4 Hz, 1H, H-2), 7.918 (bs, 1H, H-5'), 7.934 (d, J = 1.7 Hz, 1H, H-4), 8.581 (s, 1H, H-8), 11.474 (bs, 1H, NH), 11.513 (bs, 1H, CONH) ppm. ^{13}C NMR (DMSO-d_6, 150 MHz): 69.72 (CH_2), 105.76 (C-4), 111.44 (C-3), 111.98 (C-4'), 112.44 (C-7), 112.71 (C-6), 114.01 (C-3'), 124.95 (C-3a), 127.78 (C-C-4"), 128.11 (C-2" and C-6"), 128.43 (C-3" and C-5"), 130.83 (C-2), 132.15 (C-7a), 137.47 (C-1"), 145.11 (C-8), 145.34 (C-5'), 147.28 (C-1'), 153.38 (C=O), 153.77 (C-5) ppm. HRMS (ESI) *m/z*: calcd $[M+H]^+$ 360.134268; Found $[M+H]^+$: 360.13352.

N′-[(E)-(5-methoxy-1*H*-indazol-3-yl)methylidene]thiophene-2-carbohydrazide, 5l

Yield 86%; m.p. 254–255 °C. FTIR(ATR) ν_{max}: 3398 NH, 3117 NH, 1647 C=O, 1599C=N, 1586C=C; ^{1}H NMR (600 MHz, DMSO-d_6, 393 K) 1:0.15 mixture of conformers; signals for major *synperiplanar* conformer around the amide bond: δ 3.853 (s, 3H, CH_3O), 7.103 (dd, J = 2.5, 8.9 Hz, 1H, H-6), 7.214 (dd, J = 3.6, 5.00 Hz, 1H, H-4'), 7.498 (d, J = 8.9 Hz, 1H, H-7), 7.802 (d, J = 2.5 Hz, 1H, H-4), 7.828 (dd, J = 1.3, 5.0 Hz, 1H, H-3'), 8.078 (dd, J = 1.3, 3.6 Hz, 1H, H-5'), 8.649 (s, 1H, H-8), 11.373 (s, 1H, NH), 12.982 (s, 1H, NHCO) ppm. ^{13}C NMR (151 MHz, DMSO-d_6, 393 K) signals for major *synperiplanar* conformer around the amide bond: δ 55.16 (CH_3O), 101.86 (C-4), 110.71 (C-7), 119.05 (C-6), 120.10 (C-3a), 126.70 (C-4'), 130.44 (C-5'), 131.24 (C-3'), 136.04 (C-7a), 139.55 (C-3), 141.88 (C-8), 154.86 (C-5). HRMS (ESI) m/z: calcd. $[M+H]^+$ 301.075372; Found $[M+H]^+$: 301.07481.

1-Benzyl-N′-[(E)-(5-methoxy-1H-indazol-3-yl)methylidene] pyrrolidine-3-carbohydrazide, 5m

Yield 62%; m.p. 155–159 °C. FTIR(ATR) ν_{max}: 3508 NH, 3145 NH, 1661, 1636 C=O, 1606 C=N, 1583 C=C; ^{1}H NMR (DMSO-d_6, 600 MHz): 1:0.40 mixture of conformers; signals for major *synperiplanar conformer* around the amide bond: δ 2.029–2.084 (m, 1H, a-CH_2-4-H-pyrrolidine), 2.106–2.161 (m, 1H, b-CH_2-4-H-pyrrolidine), 2.415-2.476 (m, 1H, a-CH_2-5-H-pyrrolidine), 2.574 (dd, J = 7.3, 9.3 Hz, 1H, a-CH_2-2-H-pyrrolidine), 2.615-2.649 (m, 1H, b-CH_2-5-H-pyrrolidine), 3.02 (t, J = 8.9 Hz, 1H, b-CH_2-2-H-pyrrolidine), 3.55 (d, J = 13.2 Hz, 1H, a-CH_2-benzyl), 3.61 (d, J = 13.2 Hz, 1H, b-CH_2-benzyl), 3.79 (s, 3H, OCH_3), 3.800–3.848 (m, 1H, CH-3-pyrrolidine), 7.075 (dd, J = 2.4, 8.9 Hz, 1H, H-6-indazole), 7.193–7.229 (m, 1H, *p*-Ar-H), 7.282–7.292 (m, 4H, *m,o*-Ar-H), 7.485 (dd, J = 0.5, 8.9 Hz, 1H, H-7-indazole), 7.529 (dd, J = 0.5, 2.4 Hz, 1H, H-4-indazole), 8.281 (brs, 1H, CH = N), 11.336 (brs, 1H, NHCO), 13.278 (s, 1H, NH) ppm.^{13}C NMR (DMSO-d_6, 150 MHz): signals for major *synperiplanar conformer* around the amide bond: δ 26.64 (C-4-pyrrolidine), 39.78 (C-3-pyrrolidine), 53.70 (C-5-pyrrolidine), 55.03 (OCH_3), 56.60 (C-2-pyrrolidine), 59.35 (CH_2-benzyl), 100.63 (C-4-indazole), 111.73 (C-7-indazole), 118.73 (C-6-indazole), 120.19 (C-3-indazole), 126.81 (*o*-Ar-C), 128.17 (*p*-Ar-C), 128.57 (*m*-Ar-C), 136.87 (C-7a-indazole), 138.91 (CH = N), 139.14 (*ipso*-phenyl), 139.85 (C-3a-indazole), 155.02 (C-5-indazole), 174.91 (C=O). HRMS (ESI) *m/z*: calcd. $[M+H]^+$ 378.192451; Found $[M+H]^+$: 378.19173.

Antimycobacterial activity

Resazurin microtiter assay (REMA) (Martin et al. 2003; Nateche et al. 2006; Ramírez and Marquina 2017) is a colorimetric method (the results are a color reaction) to determine the minimum inhibitory concentration (MIC). A 96-well microplate was used and in each well Middlebrook 7H9 broth at different concentrations of the tested compound as well as a suspension of the reference strain *Mycobacterium tuberculosis* H37Rv (103–105 cells/ml)

Table 1 Antimycobacterial activity, in vitro cytotoxicity, selectivity index, and log *P*

Compd.	X	R^1	Ar	MIC[a] (μM)	IC_{50}[b] (μM)	SI[c]	Log *P*[d]
3a	CH	OMe		0.4412	279.5 ± 42.5	633.49	2.60
3b	CH	OMe		1.6989	211.3 ± 28.4	190.32	2.65
3c	CH	OMe		0.7431	235.4 ± 32.1	316.78	3.80
3d	CH	OMe		0.7732	198.0 ± 23.21	256.07	3.84
3e	CH	OMe		0.3969	n.d.	>1978.83	2.51
3f	CH	OMe	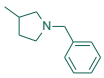	0.6640	181.4 ± 7.2	273.19	3.80
3g	CH	Br		2.7763	43.6 ± 1.1	15.70	4.88
3h	CH	Br		2.9139	136.2 ± 6.5	46.74	3.50
3i	CH	Br		2.6231	31.6 ± 4.8	12.04	4.93
3j	CH	Br		2.5300	94.7 ± 19.3	37.43	5.02
3k	CH	OCH_2Ph		0.6956	36.0 ± 2.3	51.75	4.39
5l	N	OMe		1.3247	61.6 ± 2.9	46.50	3.04
5m	N	OMe	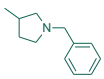	1.6648	33.9 ± 4.4	20.36	3.42
EMB.2 HCl[e]				1.6996	-	-	2.46
INH[f]				0.9115	-	-	-0.80

MIC minimum inhibitory concentration, IC_{50} half-maximal inhibitory concentration, *SI* selectivity index, *n.d.* not detected

[a]Antimycobacterial activity against reference strain of *Mycobacterium tuberculosis* H37Rv; MIC (μM) was defined as the minimum concentration of the compound required to inhibit completely the bacterial growth (0% growth)

[b]In vitro cytotoxicity to human embryonic kidney cell line HEK-293T, IC_{50} (μM)

[c]Selectivity index, SI ratio = IC_{50}/MIC

[d]Log *P* was calculated using Molecular Operating Environment of Chemical Computing Group (MOE, version 2016.08, https://www.chemcomp.com/MOE-Molecular_Operating_Environment.htm)

[e]EMB.2HCl (ethambutoldihydrochloride–reference compound)

[f]INH (isoniazid–reference compound)

were added. A parallel control contained culture medium and suspension of the reference strain, without compound. After 7 days of incubation at 37 °C, bacterial growth was measured by adding to each well the redox indicator—0.1% of resazurin. The microplate was re-incubated overnight at 37 °C; a change in color of the indicator resulting from a chemical transformation of the reagent indicated bacterial growth in the presence of the tested compound at different concentrations. The MIC was calculated and defined as the lowest concentration resulting in a complete inhibition of bacterial growth and reproduction. The MIC values are given as μM.

In vitro cytotoxicity

The cytotoxicity of selected promising agents was evaluated in the human embryonic kidney cell line HEK-293 cells (Mosmann 1983; Konstantinov et al. 1999). They were obtained from the German Collection of Microorganisms and Cell Cultures (DSMZ GmbH, Braunschweig, Germany). The cells were grown in a controlled environment—cell culture flasks at 37 °C in an incubator "BB 16-Function Line" Heraeus (Kendro, Hanau, Germany) with humidified atmosphere and 5% CO_2. The cells were reset by tripsinization and supplementation with a fresh medium two times a week. The cell lines were maintained in 90% RPMI-1640 + 10% fetal bovine serum. The cell viability was assessed using the standard MTT-dye reduction assay. In brief, exponentially growing cells were seeded in 96-well flat-bottomed microplates (100 μl/well) at a density of 2×10^4 cells per ml. After 24 h of incubation at 37 °C, they were treated with the tested compounds for 72 h. For each concentration, a set of at least 8 wells were used. After the exposure period, 10 μl MTT solution (10 mg/ml in phosphate-buffered saline (PBS)) aliquots were added to each well. Thereafter, the microplates were incubated for 4 h at 37 °C and the MTT-formazan crystals formed were dissolved through addition of 100 μl/well 5% formic acid (in 2-propanol). The absorption was measured using a Beckman Coulter DTX-800 multimode microplate reader at 580 nm. Cell survival fractions were calculated as percentage of the untreated control. In addition, half-maximal inhibitory concentration (IC_{50}) values were derived from the concentration–response curves, using non-linear regression analysis (Curve-fit, GraphPad Prism Software package).

Selectivity index (SI)

For calculation of the selectivity index, dividing the IC_{50} value by the MIC value (SI ratio = IC_{50}/MIC) for each compound, IC_{50} values from Table 1 were used.

Animals

Adult mice were kept under controlled temperature (ambient temperature 20 ± 2 °C in a 12/12 light/dark cycle). The animals were purchased from the National Breeding Centre, Slivnitsa, Bulgaria. The animals were given free access to the food diet and water. A minimum of 7-day acclimatization was allowed before the commencement of the study and their health was monitored regularly by a veterinary physician. The Vivarium (certificate of registration of farm No. 0072/01.08.2007) was inspected by the Bulgarian Drug Agency in order to check the husbandry conditions (No. A-11-1081/03.11.2011). All performed procedures were approved by the Institutional Animal Care Committee, Bulgarian Food Safety Agency, and made according to Ordinance No. 15/2006 for humaneness behavior to experimental animals.

Acute toxicity

The compound was suspended in distilled water, using 1–2 drops of Tween 80. The solution was administered via intraperitoneal (i.p.) or per oral (p.o.) route in 0.1 ml of 10 g animal body weight (b.w.). In order to decrease the number of experimental animals the acute toxicity tests after i.p. and p.o. administration of the tested compound **3e** was assessed using the simple alternative method of Schlede et al. (2005). The experiment was performed on 12 female mice: 6 of them were used for intraperitoneal administration of the tested compound and six for oral gavage. The test was started with a dose of 2000 mg/kg b.w. given i.p. to three female mice. Because of lack of toxicity or death, the same dose of 2000 mg/kg b.w. was administered to another three female mice. The animals that survived the acute administration were observed for 14 days. The same procedure was conducted for oral administration of the tested substance.

Docking evaluation

Molecular docking studies were carried out using Molecular Operating Environment (MOE, version 2016.08) of Chemical Computing Group (https://www.chemcomp.com/MOE-Molecular_Operating_Environment.htm). Docking simulations were performed on the crystal structure of *Mycobacterium tuberculosis* enoyl reductase (InhA) complexed with 1-cyclohexyl-*N*-(3,5-dichlorophenyl)-5-oxo-pyrrolidine-3-carboxamide, extracted from Protein Data Bank (http://www.rcsb.org/, PDB ID 4TZK). During the docking process, water molecules were removed while the co-factor NAD was kept. "Protonate 3D" tool of MOE was applied to pose the missing hydrogen atoms in order of the

correct ionization states to be assigned to the protein structure. "Docking" module in MOE was run to perform the molecular docking. Docking procedure has been implemented with default settings. The top 30 poses as ranked by London dG were kept and minimized using MMFF94x within a rigid receptor. The GBVI/WSA dG (Generalized-Born Volume Integral/Weighted Surface area) scoring function was then applied to score the resulting poses and 5 best poses were recorded. "Ligand Interactions" MOE tool was further used to analyze the molecular docking results by a visualization of the protein–ligand interactions in the active site of the complex. The tool presents in a diagram form an identification and visualization of the interactions between the ligand and the receptor-interacting entities, solvent molecules, and ions in the active site of the protein. Among the main interactions included are hydrogen bonds, salt bridges, hydrophobic and cation–π interactions, and solvent exposure.

Results and discussion

The synthesis of the novel series of hydrazide–hydrazones **3a–k** and **5l**, **m** was performed as outlined in Scheme 1 using an established procedure (Angelova et al. 2017a). The progress of the reaction was monitored using TLC. The novel aroylhydrazones **3a–k**, and **5l–m** were confirmed by ^{1}H NMR, ^{13}C NMR, and HRMS spectral data and their melting points. The spectral analyses were in accordance with the assigned structures. Stereochemistry was unambiguously confirmed with the help of cross-peak intensities observed in 2D NOESY (nuclear Overhauser effect spectroscopy) spectrum.

Although the four isomers were considered (Fig. S1) (Martins et al. 2014; Oliveira et al. 2017) for the aroylhydrazones with indole scaffold, *E/Z* isomerization was generally not observed and the Z geometric isomers were absent. Only the ^{1}H NMR spectrum of compound **3i** taken in DMSO-d_6 at 20 °C shows a 1:1 mixture of conformers. According to the confirmed nuclear Overhauser effect (NOE) between the methylidene proton and the NH proton, the most stable were *E* isomers around C=N double bond and the *synperiplanar* conformer around the amide O=C–N-N bond. Therefore, we concluded that a single *E* geometrical isomer was observed and the duplication pattern of novel hydrazone derivatives to be due to the presence of *syn/anti* amide conformers in DMSO-d_6. Additionally, for the purposes of structure elucidation the NMR spectra of compound **3i** were measured at 373 K to achieve a fast exchange. After cooling down to 293 K the ^{1}H NMR spectrum remained unchanged (Fig. S2). Further, the stability of compounds **3a–k** and **5l–5m** was tested by ^{1}H NMR spectra taken in DMSO-d_6 at 20 °C. All studied compounds remained unchanged for more than a month (typically stacked spectrum in Fig. S3).

The designed aroylhydrazone framework (Fig. 1) was made into two parts: indole or indazole as a mainstay and 4-phenyl-substituted aromatic rings or various heterocycles connected to hydrazide moiety to intensify the desired pharmacophoric behavior with drug-like properties and aliphatic or aromatic groups adjoined to another side (5th position) of the indole or indazole scaffold.

As can be seen, distinctions in the proposed scaffold lead to accomplished of different values of log *P* (Table 1). The in vitro evaluation of the antimycobacterial activity of the synthesized indole and indazole compounds against reference strain *Mycobacterium tuberculosis* H37Rv (Table 1) revealed that the compounds were bactericidal in nature and some of them were found to be more potent than first-line antimycobacterial drugs (isoniazid, ethambutol).

Structure–activity relationship of compounds from indole and indazole series with respect to their antitubercular activity revealed that compounds with 5-methoxy substituted indole scaffold, **3a**, **3c**, **3d**, **3e**, **3f**, and with 5-benzyloxindole scaffold **3k**, were found to be the most potent molecules with MIC values in the 0.39–0.77 µM range. Thus, the compound **3e** with 4-methyl-1,2,3-thiadiazolyl moiety and 5-metoxindole scaffold is an excellent antimycobacterial agent, the activity of which is twofold more potent than that of the isoniazid and fourfold higher than that of ethambutol. The other synthesized derivatives with the indole scaffold and a methoxy group at 5th position **3c**, **3d**, **3f**, and **3k** displayed high antimycobacterial activity equal to that of isoniazid. The replacement of phenyloxindol scaffold with methyloxindol induced a decrease in activity (compare **3a** and **3k**). On the other hand, introducing electron donating groups in aroilhydrazone moiety as *p*-methoxyphenyl **3d** or *p*-dimetilaminophenyl **3c** (as an Ar-group) does not cause a significant change in the bioactivity. Unfortunately, the activity of the derivatives with a 5-bromoindole scaffold **3g**, **3h**, **3i**, and **3j** irrespective of substitution in hydrazone moiety was weaker than that of ethambutol (compare **3b** and **3h**). Furthermore, conversion of 3-pyridyl functional group in compound **3h** into 3-indolyl in compound **3i** or 3-indolylaceto group in **3k** proved to be not effective. The compounds with indole scaffold **3b** and with indazole scaffold **5l** and **5m** showed activity, comparable to the one of the reference substance ethambutol (MIC 1.69, MIC 1.32 and 1.66 µM, respectively). However, replacing the 5-metoxindazole scaffold in a compound **5m** with 5-methoxindole scaffold in **3f** was attributed to enhanced activity, whereas the presence of a thienyl group in **5l** showed better activity in contrast to **5m**.

In order to examine the selectivity (SI) of the antiproliferative effects, the cytotoxicity of the compounds was assessed against the human embryonal kidney cell line

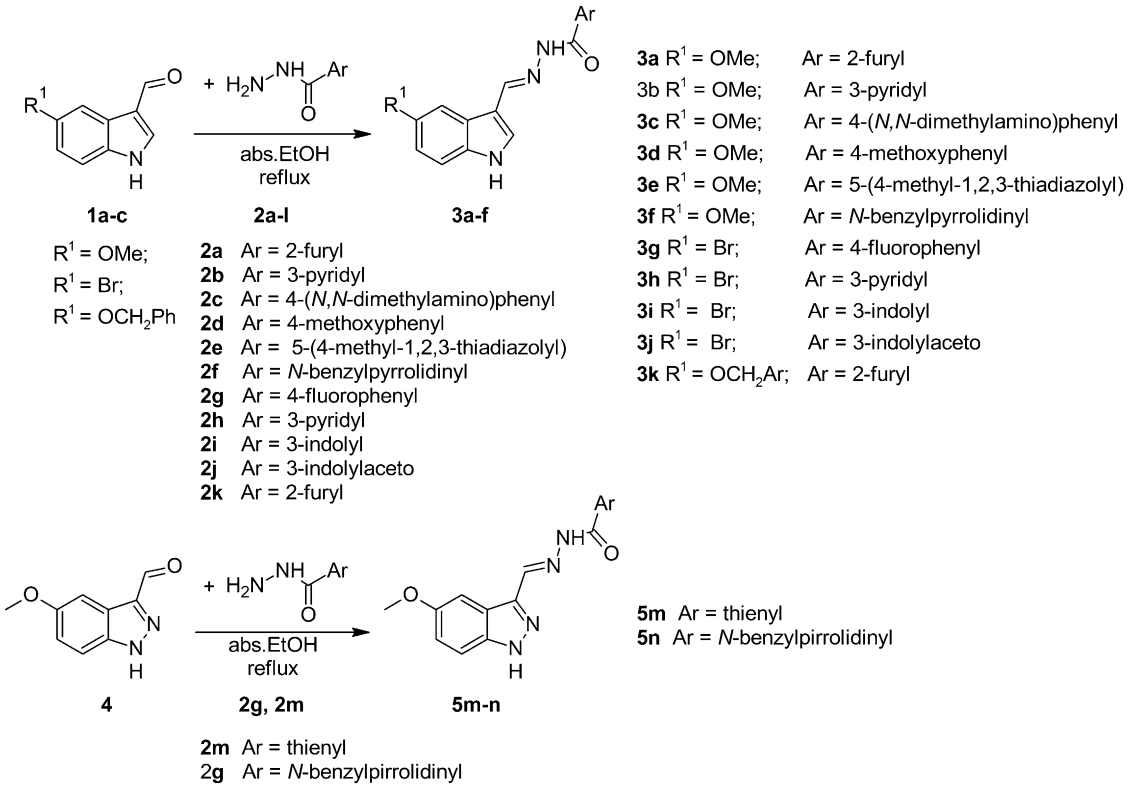

Scheme 1 The synthetic route to the preparation of the target compounds (**3a–k**, **5l**, **m**). Reaction conditions: absolute ethanol (abs. EtOH), reflux, 2 h

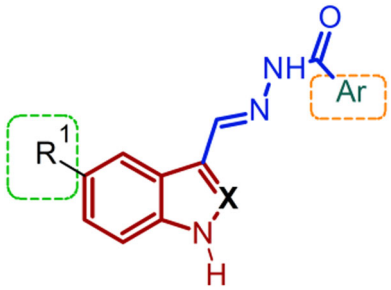

Fig. 1 Structural variations of the synthesized compounds

293T, after 72 h of exposure (Konstantinov et al. 1999; Mosmann 1983). The compounds which exhibited the highest activity **3a** and **3e** (MIC 0.44 µM and MIC 0.39 µM, respectively) were also not cytotoxic against the human embryonic kidney cells and displayed a very good selectivity index (SI = 633.49 and SI > 1978.83, respectively). The other synthesized derivatives exhibited moderate toxicity in the human embryonic kidney cell line HEK-293T. A comparison of the antimycobacterial activity of derivatives with 5-methoxindole scaffold **3a–3f** with 5-methoxindazole containing analogs **5l–5m** allows the conclusion that the compounds with indole scaffold have a better bioactivity against the *M. tuberculosis* H37Rv strain than the compounds with an 5-methoxindazole scaffold (**3f** is more active than **3m)** and showed a moderate cytotoxicity (ranging from 184.1 to 275.5 and n.d. for **3e**) as well as a very low selectivity index.

Based on the activity of **3e** (log $P = 2.51$), varying the lipophilicity (expressed in terms of log P) would have a significant effect on activity. We found that rendering the molecule as more lipophilic did not necessarily increase the antimycobacterial activity. Thus, introducing moieties which increase lipophilicity as in compounds **3k** (log $P =$ 4.39) did not improve their activity which was lower than **3a**. It appears that another property of the compounds (probably their stability) surpassed the contribution of the lipophilicity to display better antimycobacterial properties against *M. tuberculosis* H37Rv. Obviously, the more pronounced activity of nontoxic indole derivatives **3e** and **3a** can be explained by the presence of the hydrazone linker with 4-methyl-1,2,3-thiadiazolyl or furyl moieties connected to 5-metoxindole scaffold and with lower values of log P, commensurate with that of ethambutol.

Furthermore, acute toxicity for the most active compound **3e** was determined. According to the results, **3e** did not cause any mortality at the tested dose of 2000 mg/kg given i.p. No toxic reactions were noticed until day 14. No adverse effects or deaths were also noticed for oral

administration of the tested substance. For comparison, the acute toxicity of drug isoniazid for a mouse is as follows: median lethal dose (LD_{50}) (p.o.) = 176 mg/kg; LD_{50} (subcutaneous) = 160 mg/kg; LD_{50} (intramuscular) = 140 mg/kg; LD_{50} (intravenous) = 149 mg/kg (Saarstickstoff-Fatol). According to the Globally Harmonized Classification System (GSH) (http://www.chemsafetypro.com/Topics/GHS/GHS_classification_criteria_acute_toxicity_category.html) the tested compound **3e** (LD_{50} is higher than 2000 mg/kg b.w.) might be classified in class 5 (minimal hazard, between 2000 and 5000 mg/kg b.w.) or as slightly toxic, according to Hodge and Sterner scale.

To explain the activity order of **3a–k** and **5l–m** against *M. tuberculosis* H37Rv, the compounds were docked into the binding site of mycobacterial enoyl reductase (InhA). When performing docking, there are two major points to be considered when analyzing docking results: (1) the top score: the pose with the highest rank; and (2) the best pose: the pose with the lowest root mean square deviation (RMSD) to the reference ligand from the experimentally solved structure. The docking scores (Table S1 lists the essential of docking results for the synthesized compounds) of compounds **3a–k** and **5l–m** were found satisfactory in the range of −7.99 to −6.65 (Column S-score in Table S1). The results presented in Table S1 clearly indicated that compounds exhibited significant binding affinities towards the *M. tuberculosis* InhA protein. The lowest RMSD (between the pose before and after refinement) was obtained for compound **3g**, followed by **5l**, **3h**, and **3a**, while the highest rank was recorded for compound **3d**, followed by **3k**, **5m**, and **3f**. The docking score of the most active compound of the series, **3e**, was found to be −7.26. The differences in the docking scores of the compound justify the experimentally observed antimycobacterial potency of those compounds. The discrepancy between the molecular docking results and experimentally observed antimycobacterial potency of synthesized compounds might be ascribed to pharmacokinetic and biopharmaceutical properties, which ensure to a given compound better accessibility to the receptor site even when the binding interaction is a less prominent one.

Additionally, "Ligand Interactions" tool of MOE was used to obtain the protein–ligand interactions diagrams of the co-crystallized ligand of *M. tuberculosis* InhA in the ligand-binding domain (Fig. 2), as well as for the predicted binding pose in the binding site of *M. tuberculosis* InhA protein of the most active compound **3e** (Fig. 3a) and of the top score compound **3d** (Fig. 4a). Protein–ligand interactions illustrated in Figs. 2, 3a and 4a were at the maximum distance of 4.5 Å between heavy atoms of the ligand and receptor. Figures 3b and 4b demonstrate the corresponding docking conformations of compounds **3e** and **3d** with their Connolly surface.

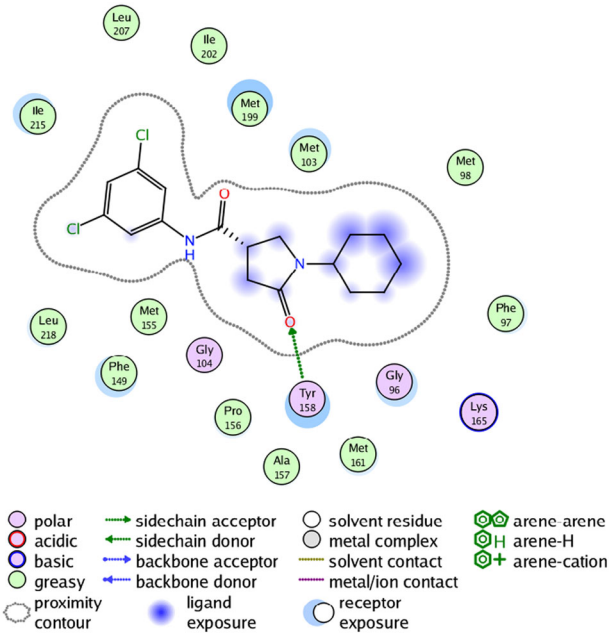

Fig. 2 Interaction diagram of the ligand-binding domain of *M. tuberculosis* InhA with 1-cyclohexyl-*N*-(3,5-dichlorophenyl)-5-oxopyrrolidine-3-carboxamide (641) (PDB ID 4TZK)

As seen from Fig. 2, only Tyr158 is involved in protein–ligand interactions. Residues Gly96, Phe97, Met103, Phe149, Met199, Ile215, and Leu218 are at receptor exposure, very close to the ligand, but still not at a binding distance. As seen from Fig. 3a (with the legend equal to that presented in Fig. 2), the most active compound **3e** demonstrated one newly appeared interaction with Phe149 (arene-H interaction) that was at receptor exposure in Fig. 2, but not exhibiting any strong interaction. Most of the residues mentioned as important were still very close. The top score pose of the compound **3d** (Fig. 4a, with the legend equal to presented in Fig. 2) repeated the interaction from Fig. 2 with Tyr158, although it is arene-H interaction instead of HB. As in the case of compound **3e**, most of the residues mentioned as important were still very close.

All synthesized compounds **3a–k** and **5l–m**, as docked in the ligand-binding domain of *M. tuberculosis* enoyl reductase complexed with 1-cyclohexyl-*N*-(3,5-dichlorophenyl)-5-oxopyrrolidine-3-carboxamide, are presented in Fig. 5 with Connolly surface.

As seen from the figure, all synthesized compounds occupied the same binding site as that of the ligand 1-cyclohexyl-*N*-(3,5-dichlorophenyl)-5-oxopyrrolidine-3-carboxamide (641), formed a cluster, and fitted well in the ligand-binding domain of *M. tuberculosis* InhA. Within the frame of this study, the docking data suggest interactions within the binding site of mycobacterial enoyl reductase that may induce the activity of the tested compounds.

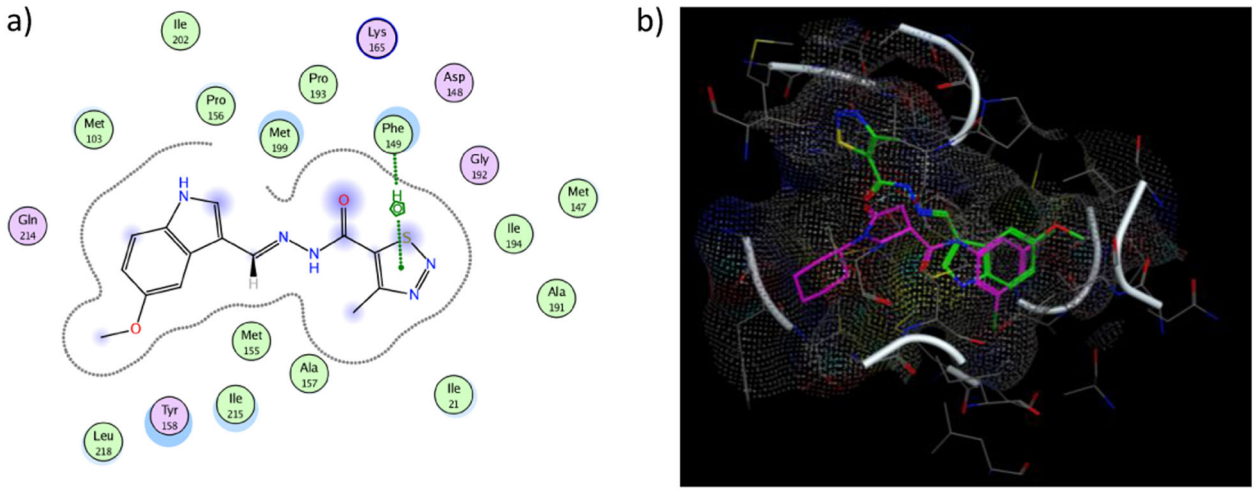

Fig. 3 Docking results for the most active compound **3e**. **a** Interaction diagrams of the ligand-binding domain of *M. tuberculosis* InhA with compound **3e**; **b** Docking conformations of compound **3e** in the active site and corresponding Connolly surface

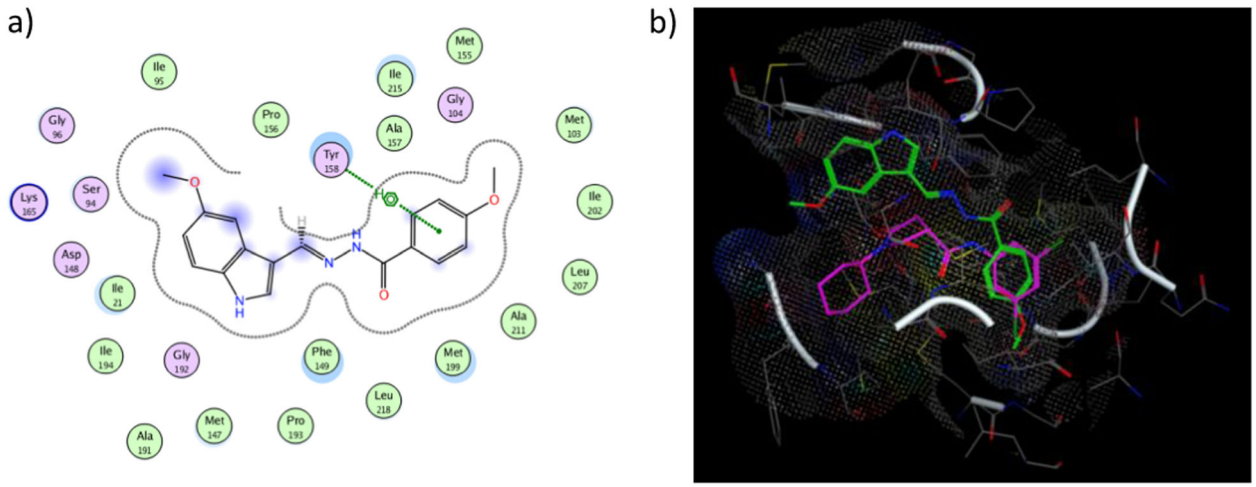

Fig. 4 Docking results for the top scored compound **3d**. **a** Interaction diagrams of the ligand-binding domain of *M. tuberculosis* InhA with compound **3d**; **b** Docking conformations of compound **3d** in the active site and corresponding Connolly surface

Conclusions

In summary, in search of different scaffolds for antitubercular agents, we have designed and synthesized two new series of substituted indole and indazol-linked hydrazide–hydrazones **3a–k** and **5l–m** in excellent yields. All compounds demonstrated significant MICs ranging from 0.39 to 2.91 μM against a referent strain *M. tuberculosis* H37Rv. The cytotoxicity against the human embryonic kidney cell line HEK-293 was also evaluated and the selectivity (SI) of the antiproliferative effects was thus assessed. All compounds displayed good SI values ranging from >1978.83 to 12.04. In general, derivatives **3a–f** and **3k** possess potent antimycobacterial activity combined with low cytotoxicity that result in SI values higher than that of their 5-bromo substituted analogs **3g–j** and of the derivatives with indazole scaffold **5l**, **m**. In addition, the probability of the most promising antimicrobial compounds to inhibit the binding cavity of *M. tuberculosis* Enoyl-ACP reductase was studied theoretically via molecular docking. The results revealed the importance of the 1,2,3-thiadiazole moiety in the connecting side chain and will help for future research in the development of novel antitubercular agents. Among the tested compounds with impressive antimycobacterial potency and selectivity, as well as very low toxicity, the hybrid of 5-metoxyindole-3-aroylhydrazone scaffold with thiadiazole moiety **3e** identified is a potentially promising candidate for developing novel selective and slightly toxic antitubercular agents with bactericidal activity.

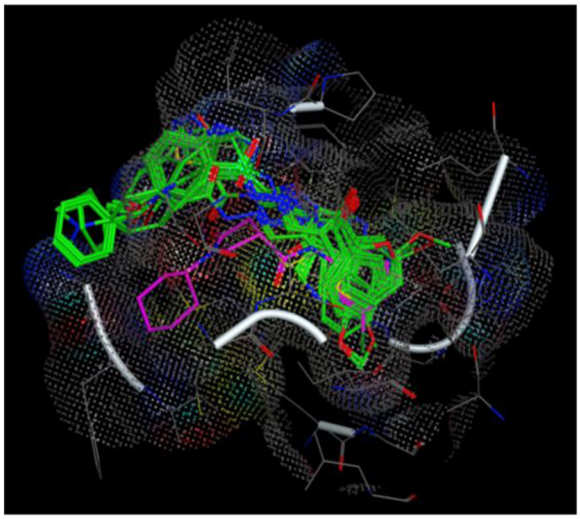

Fig. 5 Docking conformation of all synthesized compounds (in green), ligand 641 (in magenta), and corresponding Connolly surface (color figure online)

Acknowledgements This work was supported by grant contract no. 77./03.05.2018 at Medical Science Council, MU-Sofia, Bulgaria. The authors are grateful to Dr. PT Nedialkov for taking the mass spectra and to Dr. Marin Rogozerov and Dr. Javor Mitkov for the IR spectra. Acknowledgements are due to Stefka Ivanova and our student Nadezda Janakieva for their technical assistance. We would like to thank Rositsa Mihaylova for determining IC_{50} of the compounds.

Compliance with ethical standards

Conflict of interest The authors declare that they have no conflict of interest.

Ethical approval All procedures performed in studies involving animals were in accordance with the ethical standards of the institution or practice at which the studies were calculated.

Publisher's note: Springer Nature remains neutral with regard to jurisdictional claims in published maps and institutional affiliations.

References

Angelova V, Valcheva V, Vassilev N, Buyukliev R, Mihaylova R, Momekov G (2017a) Synthesis, in vitro antiproliferative and antimycobacterial activity of thiazolidine-2, 4-dione and hydantoin derivatives. Bulg Chem Commun 49:643–651

Angelova VT, Valcheva V, Pencheva T, Voynikov Y, Vassilev N, Mihaylova R, Momekov G, Shivachev B (2017b) Synthesis, antimycobacterial activity and docking study of 2-aroyl-[1] benzopyrano [4, 3-c] pyrazol-4 (1H)-one derivatives and related hydrazide-hydrazones. Bioorg Med Chem Lett 27:2996–3002

Angelova VT, Valcheva V, Vassilev NG, Buyukliev R, Momekov G, Dimitrov I, Saso L, Djukic M, Shivachev B (2017b) Antimycobacterial activity of novel hydrazide-hydrazone derivatives with 2H-chromene and coumarin scaffold. Bioorg Med Chem Lett 27:223–227

Ashok D, Gundu S, Aamate VK, Devulapally MG (2018) Conventional and microwave-assisted synthesis of new indole-tethered benzimidazole-based 1,2,3-triazoles and evaluation of their antimycobacterial, antioxidant and antimicrobial activities. Mol diversity 22:769–778

Campaniço A, Moreira R, Lopes F (2018) Drug discovery in tuberculosis. New drug targets and antimycobacterial agents. Eur J Med Chem 150:525–545

Cihan-Üstündağ G, Çapan G (2012) Synthesis and evaluation of functionalized indoles as antimycobacterial and anticancer agents. Mol Divers 16:525–539

Coelho TS, Cantos JB, Bispo ML, Gonçalves RS, Lima CH, Da Silva PE, Souza MV (2012) In vitro anti-mycobacterial activity of (E)-N'-(monosubstituted-benzylidene) isonicotinohydrazide derivatives against isoniazid-resistant strains Infect Dis Rep 4:e13

da Silva PB, Campos DL, Ribeiro CM, da Silva IC, Pavan FR (2017) New antimycobacterial agents in the pre-clinical phase or beyond: recent advances in patent literature (2001–2016). Curr Opin Ther Pat 27:269–282

Dehestani L, Ahangar N, Hashemi SM, Irannejad H, Masihi PH, Shakiba A, Emami S (2018) Design, synthesis, in vivo and in silico evaluation of phenacyl triazole hydrazones as new anticonvulsant agents. Bioorg Chem 78:119–129

Elhakeem MA, Taher AT, Abuel-Maaty SM (2015) Synthesis and anti-mycobacterial evaluation of some new isonicotinylhydrazide analogues. Bull Fac Pharm (Cairo Univ) 53:45–52

Faidallah HM, Khan KA, Rostom SA, Asiri AM (2013) Synthesis and in vitro antitumor and antimicrobial activity of some 2,3-diaryl-7-methyl-4,5,6,7-tetrahydroindazole and 3, 3a, 4, 5, 6, 7-hexahydroindazole derivatives. J Enzyme Inhib Med Chem 28:495–508

Inam A, Siddiqui SM, Macedo TS, Moreira DRM, Leite ACL, Soares MBP, Azam A (2014) Design, synthesis and biological evaluation of 3-[4-(7-chloro-quinolin-4-yl)-piperazin-1-yl]-propionic acid hydrazones as antiprotozoal agents. Eur J Med Chem 75:67–76

John SF, Aniemeke E, Ha NP, Chong CR, Gu P, Zhou J, Zhang Y, Graviss EA, Liu JO, Olaleye OA (2016) Characterization of 2-hydroxy-1-naphthaldehyde isonicotinoyl hydrazone as a novel inhibitor of methionine aminopeptidases from Mycobacterium tuberculosis. Tuberc (Edinb) 101:S73–S77

Konstantinov SM, Eibl H, Berger MR (1999) BCR-ABL influences the antileukaemic efficacy of alkylphosphocholines. Br J Haematol 107:365–374

Malapati P, Krishna VS, Dharmarajan S (2018) Identification and development of novel indazole derivatives as potent bacterial peptidoglycan synthesis inhibitors. Int J Mycobact 7:76

Martin A, Camacho M, Portaels F, Palomino JC (2003) Resazurin microtiter assay plate testing of Mycobacterium tuberculosis susceptibilities to second-line drugs: rapid, simple, and inexpensive method. Antimicrob Agents Chemother 47:3616–3619

Martins F, Santos S, Ventura C, Elvas-Leitão R, Santos L, Vitorino S, Reis M, Miranda V, Correia HF, Aires-de-Sousa J (2014) Design, synthesis and biological evaluation of novel isoniazid derivatives with potent antitubercular activity. Eur J Med Chem 81:119–138

Mosmann T (1983) Rapid colorimetric assay for cellular growth and survival: application to proliferation and cytotoxicity assays. J Immunol Methods 65:55–63

Nateche F, Martin A, Baraka S, Palomino JC, Khaled S, Portaels F (2006) Application of the resazurin microtitre assay for detection of multidrug resistance in *Mycobacterium tuberculosis* in Algiers. J Med Microbiol 55:857–860

Negatu DA, Liu JJ, Zimmerman M, Kaya F, Dartois V, Aldrich CC, Gengenbacher M, Dick T (2017) Whole cell screen of fragment library identifies gut microbiota metabolite indole propionic acid as antitubercular. Antimicrob Agents Chemother 62: e01571–17

North J, Jackson MC (2018) Indole-based therapeutics. U.S. Patent Application No. 15/669,289.

Nyantakyi SA, Li M, Gopal P, Zimmerman M, Dartois V, Gengenbacher M, Dick T, Go M-L (2018) Indolyl Azaspiroketal Mannich bases are potent anti-mycobacterial agents with selective membrane permeabilizing effects and in vivo activity. J Med Chem 61:5733–5750

Oliveira PF, Guidetti B, Chamayou A, André-Barrès C, Madacki J, Korduláková J, Mori G, Orena BS, Chiarelli LR, Pasca MR (2017) Mechanochemical synthesis and biological evaluation of novel isoniazid derivatives with potent antitubercular activity. Molecules 22:1457

Parlar S, Erzurumlu Y, Ilhan R, Ballar Kırmızıbayrak P, Alptüzün V, Erciyas E (2018) Synthesis and evaluation of pyridinium-hydrazone derivatives as potential antitumoral agents. Chem Biol Drug Des 92:1198–1205

Park Y, Pacitto A, Bayliss T, Cleghorn LA, Wang Z, Hartman T, Arora K, Ioerger TR, Sacchettini J, Rizzi M (2016) Essential but not vulnerable: indazole sulfonamides targeting inosine monophosphate dehydrogenase as potential leads against Mycobacterium tuberculosis. ACS Infect Dis 3:18–33

Peng H-N, Ye L-M, Zhang M, Yang Y-C, Zheng J (2018) Synthesis and antimicrobial activity of 3, 4-dihydropyrimidin-2 (1H)-one derivatives containing a hydrazone moiety. Heterocycl Commun 24:113–117

Poma A, Fontecchio G, Carlucci G, Chichiricco G (2012) Antiinflammatory & anti-allergy agents in medicinal chemistry. Anti-Inflamm Anti-Allergy Agents Med Chem 1:37–51

Popiołek Ł, Biernasiuk A (2017) New hydrazides and hydrazide-hydrazones of 2, 3-dihalogen substituted propionic acids: synthesis and in vitro antimicrobial activity evaluation Chem Biodivers 14:e1700075

Popiołek Ł, Biernasiuk A, Berecka A, Gumieniczek A, Malm A, Wujec M (2018) New hydrazide–hydrazones of isonicotinic acid: synthesis, lipophilicity and in vitro antimicrobial screening. Chem Biol Drug Des 91:915–923

Ragavendran JV, Sriram D, Patel SK, Reddy IV, Bharathwajan N, Stables J, Yogeeswari P (2007) Design and synthesis of anticonvulsants from a combined phthalimide–GABA–anilide and hydrazone pharmacophore. Eur J Med Chem 42:146–151

Ramírez A, Marquina MA (2017) Aspectos clínicos y microbiológicos de las infecciones producidas por el complejo Mycobacterium abscessus. Av En Biomed 6:120–132

Rudavath D, Sreenivasulu R, Raju RR (2018) Synthesis and antitumor evaluation of indole-substituted indole-fused keto hydrazide–hydrazones. J Pharm Res (Mohali, India) 12:42–46

Schlede E, Genschow E, Spielmann H, Stropp G, Kayser D (2005) Oral acute toxic class method: a successful alternative to the oral LD50 test. Regul Toxicol Pharmacol 42:15–23

Şenkardeş S, Kaushik-Basu N, Durmaz I, Manvar D, Basu A, Atalay R, Küçükgüzel ŞG (2016) Synthesis of novel diflunisal hydrazide–hydrazones as anti-hepatitis C virus agents and hepatocellular carcinoma inhibitors. Eur J Med Chem 108: 301–308

Shirinzadeh H, Altanlar N, Yucel N, Ozden S, Suzen S (2011) Antimicrobial evaluation of indole-containing hydrazone derivatives. Z Naturforsch C 66:340–344

Velezheva V, Brennan P, Ivanov P, Kornienko A, Lyubimov S, Kazarian K, Nikonenko B, Majorov K, Apt A (2016) Synthesis and antituberculosis activity of indole–pyridine derived hydrazides, hydrazide–hydrazones, and thiosemicarbazones. Bioorg Med Chem Lett 26:978–985

Vidyacharan S, Adhikari C, Krishna VS, Reshma RS, Sriram D, Sharada DS (2017) A robust synthesis of functionalized 2H-indazoles via solid state melt reaction (SSMR) and their antitubercular activity. Bioorg Med Chem Lett 27:1593–1597

World Health Organization (2018) Global tuberculosis report 2017. World Health Organization, Geneva.

Yang T, Moreira W, Nyantakyi SA, Chen H, Aziz DB, Go M-L, Dick T (2017) Amphiphilic indole derivatives as antimycobacterial agents: structure–activity relationships and membrane targeting properties. J Med Chem 60:2745–2763

Yurttaş L, Ertaş M, Cankılıç MY, Demirayak Ş (2017) Synthesis and antimycobacterial activity evaluation of isatin-derived 3-[(4-aryl-2-thiazolyl])hydrazone]-1H-indol-2, 3-diones. Acta Pharm Sci 55:51–58